

## Light-lanthanide impurities in iridium: From nonmagnetic $4f$ states to large local magnetic moments

Lars Nordström and Börje Johansson

*Condensed Matter Theory Group, Department of Physics, University of Uppsala, Box 530, S-751 21 Uppsala, Sweden*

(Received 21 June 1991)

An investigation of the magnetic properties of the light lanthanides Ce, Pr, Nd, and Pm as impurities in face-centered-cubic iridium metal has been performed by means of the linear-muffin-tin-orbital-Green's-function method. In agreement with experiment, Ce and Pr were found to be nonmagnetic while Nd and Pm were found to have large magnetic moments composed of both a spin part and an orbital part. An analysis of the mechanism responsible for the nonmagnetic solutions is given. The importance of the hybridization between the impurity  $4f(t_{2u})$  states and the  $5d$  states of the surrounding host atoms is stressed.

### I. INTRODUCTION

Whether an impurity of a transition-metal element or a rare-earth element forms a magnetic moment or not in a metal host is a question with a long history, the answer to which is not yet completely settled. Anderson proposed a simple model<sup>1</sup> in 1961 where a virtual bound state on the impurity atom is formed through mixing with the conduction bands of the host, and showed that, in the Hartree-Fock approximation, there are both magnetic and nonmagnetic solutions, depending on the parameters of the model. Since then this model has been applied to a variety of systems. Besides the systems of  $3d$  transition elements in various hosts, which was the problem originally addressed by Anderson, most attention has probably been given to Ce impurities.<sup>2</sup> It has been shown that, in the exact solution of the Anderson model, there is generally a nonmagnetic solution (the so-called Kondo singlet) at low temperatures, but a magnetic solution may occur at higher temperatures (above the so-called Kondo temperature).<sup>3</sup> However, the approximation of a shapeless conduction-band density of states adopted within the Anderson model is not always appropriate, especially not when the host has band states of  $d$  or  $f$  character. Then, instead of a single  $s$  band, there are several bands which are far from free-electron-like and have quite complicated dispersions. As a consequence, the host density of states (DOS) shows a lot of structure, and it is not obvious how this will influence on the impurity level.

*Ab initio* calculations for  $3d$  impurities in noble metals or transition metals have shown that the hybridization between the  $d$  states of the host and the  $d$  levels of the impurity are important for a proper description of these systems.<sup>4-6</sup> These calculations, which were performed within the local-density approximation (LDA) to the density-functional theory, failed, however, to achieve a nonmagnetic Kondo singlet at zero temperature, in the same way as the Hartree-Fock solution to the Anderson model fails in this respect. The results were, however, consistent with available experiments as regards the size of the magnetic moments.

The nature of the  $4f$  states in cerium metal and several cerium compounds is controversial. On one hand, the electronic structure of the nonmagnetic ( $\alpha$ -like) Ce systems is viewed upon as if the  $4f$  states together with conduction states form a coherent Kondo singlet.<sup>2</sup> In the so-called Kondo volume collapse model,<sup>7</sup> a volume dependence of the binding energy for the singlet state provides the mechanism for the isostructural  $\alpha$ - $\gamma$  transition in the cerium metal. On the other hand, a model has been proposed where the  $4f$  states are considered to be itinerant in some cerium systems, e.g.,  $\alpha$ -Ce and CeNi<sub>2</sub>, but localized in other systems, e.g.,  $\gamma$ -Ce and CeCu<sub>2</sub>. In this model the  $\alpha$ - $\gamma$  transition corresponds to a Mott transition of the  $4f$  states.<sup>8</sup> In electronic structure calculations<sup>9,10</sup> for Ce metal, the dispersion of the  $f$  bands is found to originate both from a direct overlap of  $4f$  orbitals at neighboring sites and an overlap between the  $4f$  orbital and  $5d$  orbitals centered on the surrounding sites, i.e., the  $4f$  states hybridize with the  $5d$  conduction band. Since the Ce-Ce distances are generally larger in intermetallic compounds than for the pure metal, the  $4f$ - $4f$  overlap decreases in importance and the dominant factor for the width of the  $f$  band is due to  $4f$  hybridization with the ligand states.

To obtain a further understanding of cerium systems, it is suitable to examine cerium impurities dissolved into different hosts, where no direct  $4f$ - $4f$  overlap is possible. Transition-metal hosts with  $d$  bands that can mix with  $4f$  states are especially interesting. A thorough experimental investigation of the magnetic properties of cerium in different hosts by means of the perturbed-angular- $\gamma$ -ray-distribution (TDPAD) technique has been performed by Riegel *et al.*<sup>11</sup> In this series of experiments it was found that, depending on the host, the full range of behavior from nonmagnetic to fully developed Russell-Saunders coupled moments can be achieved for cerium impurities, and even for some of the other light lanthanide impurities.

As regards theoretical work, besides the extensive work within the Anderson model, *ab initio* calculations for the electronic structure of Ce dissolved in Cu, Ag,

and Pd have been reported.<sup>12</sup> In this study cerium was found to be nonmagnetic in palladium and to possess a magnetic moment in the noble metal hosts, in agreement with experiments.

In the present paper we report an *ab initio* electronic structure calculations, utilizing the Green's-function linear-muffin-tin-orbital (LMTO) scheme, for the light lanthanides Ce, Pr, Nd, and Pm as impurities in Ir. This metal host is extreme in the sense that iridium has a small equilibrium volume, which then will act as a huge "chemical pressure" on the comparatively large, dissolved lanthanide atoms. Experimentally<sup>13,14</sup> it has been claimed that, while Nd and Pm form magnetic moments, Ce and Pr are nonmagnetic in this small volume host. It is our purpose here to calculate the magnetic properties of these impurity systems and see if the experimental findings can be understood within the realm of our calculations. The present authors have earlier made an investigation of these systems utilizing a supercell approach to the impurity problem.<sup>15</sup> That approach had its drawbacks due to the limited size of the super cell and therefore we now reinvestigate this problem with a more appropriate technique. The method we use is reviewed in Sec. II and the results are presented in Sec. III. In Sec. IV, a more thorough discussion of the mechanism responsible for the nonmagnetic ground state found for Ce and Pr is given. The nature of the local magnetic moments of Nd and Pm is investigated further by means of calculations including the so-called orbital polarization.<sup>16</sup> The results of these calculations are discussed in Sec. V. Finally, in Sec. VI, a summary of the present work is given.

## II. COMPUTATIONAL METHOD

The electronic structure of the host-impurity system is calculated by means of a Green's-function technique<sup>17</sup> within the linear-muffin-tin-orbital method<sup>18</sup> in the atomic sphere approximation (ASA) and in its orthogonal representation. This technique has been described in detail before but is here briefly reviewed to outline the premises for the subsequent analysis of the results.

Firstly, the Green's-function matrix of the unperturbed crystal (i.e., without impurity),  $G^0(E)$ , is calculated from the result of a self-consistent LMTO calculation. Then the Green's-function matrix of the perturbed system with the impurity  $G(E)$  may be calculated through a Dyson equation,

$$G(E) = G^0(E) - G^0(E)\Delta V G(E). \quad (1)$$

Here and onwards quantities are written as matrices in the space spanned by the LMTO basis set, with the implicit composite indices  $i = (R, lm, \sigma)$ .  $R$  stands for the atomic site,  $l$  the azimuthal quantum number,  $m$  the magnetic quantum number, and  $\sigma$  the spin.  $\Delta V = V - V_0$  is the change in the potential induced by the impurity. Since  $\Delta V$  is not known, Eq. (1) has to be solved by iteration. From the solution of Eq. (1), together with the wave functions  $\phi_i(E, r)$  obtained from the Schrödinger-like one-electron equation with the potential  $V(r)$ , spherically averaged, valence charge and magnetization densi-

ties,  $n_{v,R}(r)$  and  $m_{v,R}(r)$ , are constructed,

$$n_{v,R}(r) = (4\pi)^{-2} \text{Tr} \int^{E_F} [\phi(E, r)]^2 \text{Im} G(E) dE, \quad (2a)$$

$$m_{v,R}(r) = (4\pi)^{-2} \text{Tr} \sigma \int^{E_F} [\phi(E, r)]^2 \text{Im} G(E) dE, \quad (2b)$$

where  $E_F$  is the Fermi energy. The trace in Eqs. (2a) and (2b) is to be taken only over the indices  $l, m$ , and  $\sigma$  of the matrices and  $\phi(E, r)$  is viewed as a diagonal matrix. Here the close relationship between the density of states and the imaginary part of the Green's function,  $N(E) = \text{Im} G(E)/\pi$ , has been used. From these densities a potential  $V(r)$  is constructed through the local-density approximation and inserted into Eq. (1). This procedure is repeated until convergence is achieved.

With a simple scaling, the Korringa-Kohn-Rostoker-ASA (KKR-ASA) Green's function  $g(E)$  is obtained from the Hamiltonian Green's function  $G(E)$ ,

$$g(E) = \Delta^{1/2} G(E) \Delta^{1/2}. \quad (3)$$

A Dyson equation for  $g(E)$  is then readily derived from Eq. (1),

$$[1 + g^0(E)\Delta P(E)]g(E) = g^0(E), \quad (4)$$

where the perturbation is now represented by the change  $\Delta P(E)$  of the parametrized potential function  $P(E) = (E - C)/\Delta$ . Here and in Eq. (3),  $C$  and  $\Delta$  are so-called potential parameters commonly utilized within the LMTO method.

In practice, the Dyson equation for  $g(E)$ , Eq. (4), is solved instead of Eq. (1). The dimension of this matrix equation is proportional to the range of  $\Delta P(E)$ . For most problems it is sufficient to include the perturbation for the impurity site and its nearest neighbors. With the help of group theory, the matrix equation may be reduced into equations of lower dimensions, one equation for each of the irreducible representations. In the present case of iridium with a cubic crystal (fcc), the point-group symmetry is  $O_h$ , for which there are ten irreducible representations. On the perturbed impurity site, in fact, only six are needed to represent the Green's-function matrix when angular momenta up to three are included. Of these, only  $t_{1u}$  contains a basis function from different angular momenta ( $p$  and  $f$ ). The other five stem from a unique angular momentum. For the  $f$  states, which are the states in focus in this paper, there are three different representations, the one-dimensional representation  $a_{2u}$  and the two three-dimensional representations  $t_{1u}$  and  $t_{2u}$ .

The calculations were performed for a fcc crystal at the experimental lattice constant,<sup>19</sup> 3.84 Å. The effective potentials were constructed within the LDA with the parametrization of von Barth and Hedin<sup>20</sup> for the exchange and correlation parts. On all atoms, basis functions with angular momenta up to three were included.

## III. RESULTS

Figure 1 shows the theoretical local density of states for cerium and praseodymium as impurities in iridium together with the DOS of the unperturbed host. The most pronounced feature in the impurity DOS is the sharp  $f$

peak situated above the Fermi level. This peak is considerably closer to the Fermi level for Pr than for Ce. There is, however, also  $f$  character below the Fermi level in a tail reaching quite far down from the peak position. This structure has been produced by the mixing of the  $f$  level of the impurity with the  $5d$  bands of the host in a way that we will describe in more detail in Sec. IV. Since the Fermi level is below the rapidly raising part of the peak for both Ce and Pr, there is not enough DOS at the Fermi level to favor spin polarization. For Nd and Pm as impurities, the peak position is found at an even lower energy. This is due to the increased nuclear charge and the increased  $f$  occupation number, which brings the Fermi level into regions with high  $4f$  DOS, and therefore the system is unstable towards formation of a local magnetic moment.

The basic results from the nonmagnetic calculations are collected in Table I. The obtained  $4f$  occupation

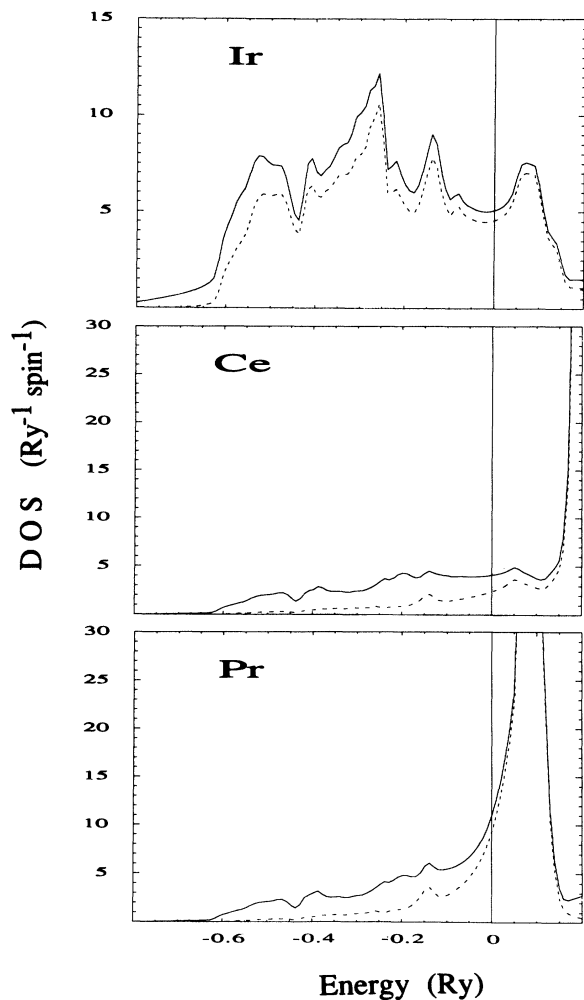


FIG. 1. The total local density of states for the Ir host and for Ce and Pr as impurities. Shown with dashed lines are the angular momentum projected DOS for Ir  $5d$  and Ce or Pr  $4f$  states. The Fermi level is at zero energy.

TABLE I. Calculated occupation numbers and charges for lanthanide impurities in iridium metal obtained from a nonmagnetic one-site calculation.  $n_l$  is the occupation number for angular momentum  $l$ .  $q$  is the charge of the impurity atom in units of  $e$ .

Atom	Ce	Pr	Nd	Pm
$n_{sp}$	0.696	0.727	0.750	0.818
$n_d$	1.830	1.839	1.839	1.785
$n_f$	1.048	2.024	3.031	4.049
$q$	0.426	0.410	0.381	0.348

numbers are very close to integer values, which increases from one for cerium to four for promethium in steps by one. The  $s$ ,  $p$ , and  $d$  occupation numbers stay almost constant through the series. However, the sum of them reflects a tendency of a decrease in electron transfer from the impurity to the host as one goes to heavier lanthanides. This has most likely the same origin as the well-known lanthanide contraction. The localized  $4f$  electrons screen the nuclear charge experienced by the more extended  $s$ ,  $p$ , and  $d$  states. However, this screening is not perfect and therefore the effective nuclear charge increases slightly through the lanthanide series which causes a contraction of the  $s$ ,  $p$ , and  $d$  states.

As mentioned above, the nonmagnetic solutions are unstable for Nd and Pm as impurities, in accordance with the experimental data. In Fig. 2, the spin-polarized local DOS for the two atom types is shown and in Table II the main results from the spin-polarized calculations are collected. The spin-up and spin-down  $f$  peaks in the local DOS are split far apart which results in appreciable  $4f$  magnetic spin moments of  $1.44\mu_B$  and  $2.98\mu_B$  for Nd and Pm, respectively.

In the calculations above, only the potential at the impurity site has been allowed to change. To investigate how reliable this approximation is, calculations have been performed where the potentials at the nearest-neighbor shell are also allowed to vary. The results from these calculations are collected in Table III. From a comparison between these data and those in Tables I and II, one notices that the one-site approximation in certain respects is

TABLE II. Occupation numbers and charges for Nd and Pm as impurities in iridium metal obtained from a spin-polarized one-site calculation.  $n_l$  is the occupation number for the angular momentum  $l$ .  $q$  is the charge of the impurity atom in units of  $e$ .  $M_f$  and  $M_{tot}$  are the  $4f$  projected and total magnetic moments of the impurity atom (in units of  $\mu_B$ ), respectively.

Atom	Nd	Pm
$n_{sp}$	0.748	0.818
$n_d$	1.834	1.780
$n_f$	3.036	4.061
$q$	0.382	0.341
$M_f$	1.439	2.983
$M_{tot}$	1.472	3.034

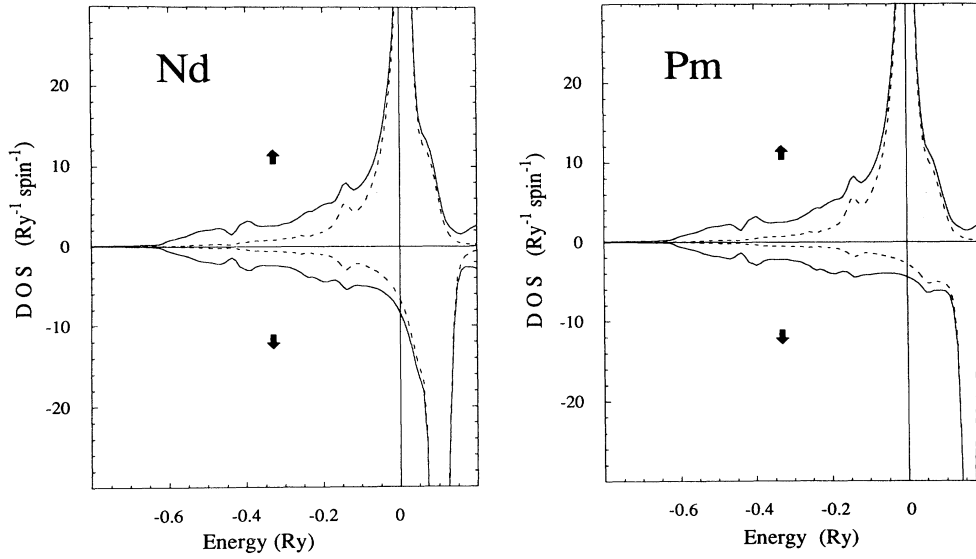


FIG. 2. Spin-projected local DOS for Nd in Ir and Pm in Ir. The majority (minority) spin states are shown in the upper (lower) panel. The  $4f$  DOS are also plotted (dashed lines).

not very good. The electron transfer away from the impurity is almost doubled in the two-shell calculation, which is also reflected in the  $f$  count which is decreased. This electron deficiency within the impurity sphere is actually overcompensated by the shell of nearest neighbors, resulting in a total excess of electrons in the perturbed area. The problems of getting the perturbed volume neutral could be solved, in principle, by permitting the potentials of more shells to change until neutrality is achieved. The neglect of volume expansion around the impurity site is, however, probably an even more serious deficiency of the present treatment and is very hard to avoid. In order to estimate the influence of the volume expansion, we have performed a calculation for Pr as an impurity in a host with an expanded volume. Such a calculation certainly overestimates the overall effect of a lo-

cal lattice expansion around the large impurity atom, but it is one way to see how a larger nearest-neighbor distance influences the electronic states of the impurity. Pr is found to remain nonmagnetic in a host with 5% larger lattice constant. This gives some credibility to the conclusions drawn from the results of the calculation with an unrelaxed host crystal.

From the calculations where the potentials of the nearest neighbors are also allowed to relax it is found that the magnetic moments for Nd and Pm are underestimated in the one-site approximation. However, the magnetization density is well localized on the impurity site, as can be seen from the fact there are only  $-0.02\mu_B$  on the atoms in the neighboring shell. This, together with the fact that the onset of formation of local magnetic moments are correctly described in the one-site approximation, lead us to the conclusion that, for the accuracy needed here, the one-site approximation is sufficient for our present purposes. This also considerably simplifies the analysis of the calculations.

To get a clearer picture of the nature of the  $f$  states, we divide them into their symmetry representations. Figure 3 shows the local DOS for the  $t_{2u}$  states and the sum of the local DOS for the  $a_{2u}$  and  $t_{1u}$  states for Ce and Pr as

TABLE III. Occupation numbers and charges for lanthanide impurities in iridium metal obtained from two-shell calculations.  $n_f$  is the occupation number for angular momentum  $l=3$ .  $q_{\text{imp}}$  and  $q_{\text{tot}}$  are the charges of the impurity atom and the whole perturbed region, respectively, in units of  $e$ .  $M_{\text{imp}}$ ,  $M_f$ , and  $M_{\text{NN}}$  are the total and  $f$ -projected magnetic moments for the impurity atom and the total magnetic moment of a nearest-neighbor Ir atom, respectively, in units of  $\mu_B$  per atom.

Atom	Pr	Nd	Pm
$n_f$	1.935	2.937	3.935
$q_{\text{imp}}$	0.664	0.732	0.636
$q_{\text{tot}}$	-0.323	-0.790	-0.659
$M_f$		1.541	3.029
$M_{\text{imp}}$		1.575	3.067
$M_{\text{NN}}$		-0.025	-0.024

TABLE IV. Calculated  $f$  occupation numbers divided into the different symmetry representations of the cubic point group.

Atom	Ce	Pr	Nd	Pm
$n(a_{2u})$	0.086	0.103	0.110	0.122
$n(t_{1u})$	0.285	0.472	0.711	1.086
$n(t_{2u})$	0.667	1.419	2.210	2.841

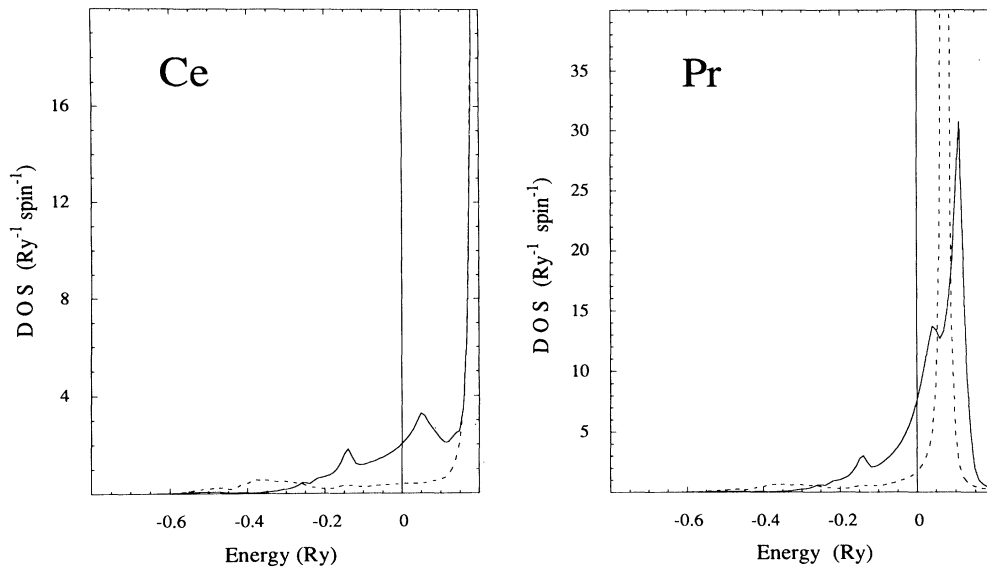


FIG. 3. Local  $4f$  DOS divided into  $t_{2u}$  (solid line) symmetry and  $a_{2u}$  and  $t_{1u}$  (dashed line) symmetries, for Ce and Pr as impurities in iridium metal. The Fermi level is at zero energy.

impurities. The  $a_{2u}$  and the  $t_{1u}$  states were found to be almost indistinguishable, the peak of the  $a_{2u}$  states is only slightly narrower but coincide exactly in energy with the peak of the  $t_{1u}$  states. Therefore, we only plot the sum of the two for the benefit of visuality. Especially for Pr it is clear that the states with  $t_{2u}$  symmetry have quite a different shape than the other two. While the  $a_{2u}$  and  $t_{1u}$

states have a very sharp peak situated 0.07 Ry above the Fermi level, the  $t_{2u}$  states are smeared out over a range of 0.4 Ry with three distinct peaks. The former case we will denote as a resonance or a virtual bound state, while the latter case we will attribute to a particularly strong hybridization of the  $4f$  states with states of the neighboring sites. The reason for this will be discussed in some depth

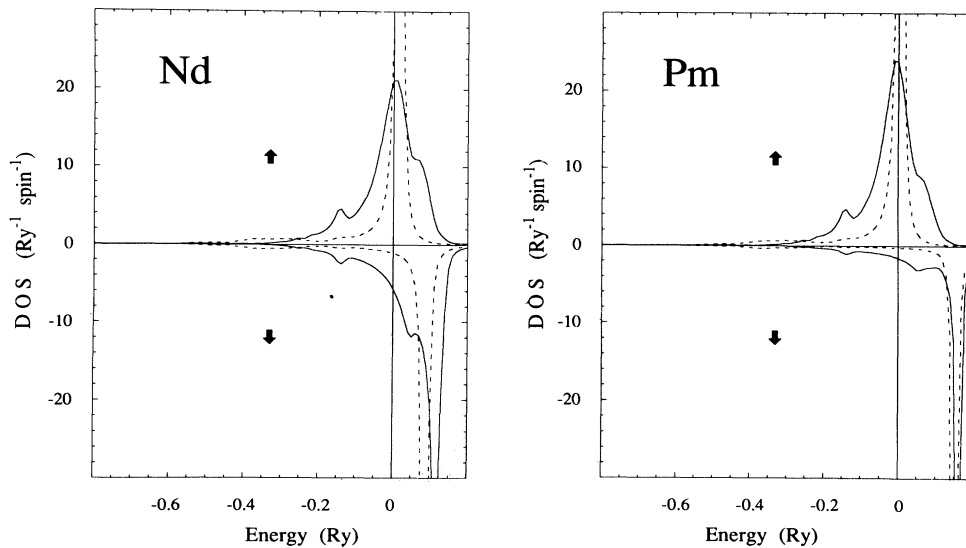


FIG. 4. Spin-projected local  $4f$  DOS divided into  $t_{2u}$  (solid line) symmetry and  $a_{2u}$  and  $t_{1u}$  (dashed line) symmetries, for Nd and Pm as impurities in iridium metal. The majority (minority) spin states are plotted in the upper (lower) panel. The Fermi level is at zero energy.

TABLE V. Spin-projected  $f$  occupation numbers for the different representations of the cubic point group.

Atom spin	Nd		Pm	
	↑	↓	↑	↓
$n(a_{2u})$	0.069	0.046	0.344	0.039
$n(t_{1u})$	0.660	0.193	1.419	0.141
$n(t_{2u})$	1.508	0.560	1.759	0.358

in the next section. In the case of Ce, the  $t_{2u}$  states have a similar shape as those of Pr, but the third peak, the one with highest energy, coincide in energy with the resonance and have a magnitude which by far dominates over the other two peaks.

For Ce and Pr the resonance peak is situated above the Fermi energy and the only occupation of the  $a_{2u}$  and  $t_{1u}$  states is due to a very narrow tail reaching down below  $E_F$ . Therefore, the dominant part of the  $f$  occupation number stems from the  $t_{2u}$  symmetry, as can be seen in Table IV. In this table the occupation numbers are also shown for the nonmagnetic calculations of Nd and Pm. From these one finds that the resonance peak is lowered in energy and becomes somewhat more populated when the atomic number increases, although the  $a_{2u}$  states, which, as already mentioned, are slightly narrower than the  $t_{1u}$  states, remain essentially unoccupied. However, for the nonmagnetic state, the gradual filling of the  $f$  shell when we proceed from Ce to Pm, mainly takes place in the  $t_{2u}$  state.

The spin-polarized calculations give a similar picture, Fig. 4 and Table V. The  $t_{2u}$  states are broad while the states of the two other types have a sharp resonance. However, the resonance for the majority spin is situated at the Fermi level which causes an appreciable occupation also for the  $a_{2u}$  and  $t_{1u}$  states. Therefore, when we proceed from Nd to Pm, the additional  $f$  electron goes mainly into the resonance state, in contrast to the situation for the nonmagnetic case.

#### IV. RESONANCES AND HYBRIDIZATION

From Fig. 3 one notices that the  $t_{2u}$  states, on one hand, and the  $a_{2u}$  and  $t_{1u}$  states, on the other, are evidently of different nature. In order to elucidate the origin of this difference, we will compare the  $t_{2u}$  and the  $a_{2u}$  symmetry states for the case of Pr as impurity. Firstly, due to the simplification of the one-site approximation, the Dyson equation for these two symmetry representations,  $\alpha$ , can be written in a simple scalar form

$$g_\alpha(E) = \frac{g_\alpha^0(E)}{1 + \Delta P_l(E) g_\alpha^0(E)}. \quad (5)$$

For the  $t_{2u}$  representation, there is, of course, a threefold degeneracy in  $g_\alpha(E)$ . The scalar form is due to the choice of cubic harmonics as basis functions within the irreducible representations in which the  $g_\alpha$  matrices are

diagonal. Then, for the imaginary part, which is what enter the local DOS, we find

$$\text{Im}g_\alpha(E) = \frac{\text{Im}g_\alpha^0(E)}{[Q_\alpha(E)]^2 + [\Delta P_l(E) \text{Im}g_\alpha^0(E)]^2}, \quad (6a)$$

where

$$Q_\alpha(E) = 1 + \Delta P_l(E) \text{Re}g_\alpha^0(E). \quad (6b)$$

From Eq. (6), a resonance in  $\text{Im}g_\alpha$  will occur for an energy where first of all  $Q_\alpha(E) = 0$  and secondly  $\text{Im}g_\alpha^0$  is small.<sup>21</sup> For energies close to such a resonance energy,  $E_R$ , we get from an expansion of Eq. (6a),

$$\text{Im}g_\alpha(E) = \frac{A^{-2} \text{Im}g_\alpha^0(E)}{(E - E_R)^2 + (B/A)^2}, \quad (7)$$

where

$$A = \left[ \frac{\partial}{\partial E} (\Delta P_l \text{Re}g_\alpha^0) \right]_{E=E_R}, \quad (8a)$$

$$B = \Delta P_l(E_R) \text{Im}g_\alpha^0(E_R). \quad (8b)$$

Hence,  $\text{Im}g_\alpha(E)$  takes a Lorentzian shape around  $E_R$ , which is representative for a virtual bound state. Only the presence of host states of the right local symmetry at the energy  $E_R$  prevents a bound state to be formed. The width of the resonance may be viewed as determined by the weak hybridization between the localized states at the impurity and the host states of the same symmetry. However, we avoid this terminology to use the concept of hybridization for the competing mechanism discussed below.

In Fig. 5 we have plotted the functions  $Q_\alpha(E)$  and  $\text{Im}g_\alpha^0(E)$  together with  $\text{Im}g_\alpha(E)$  for the states with  $a_{2u}$  and  $t_{2u}$  symmetry. It is clear that the conditions for a resonance are fulfilled for the  $a_{2u}$  states at an energy 0.07 Ry above  $E_F$ . For the  $t_{2u}$  states, however, the conditions are not at all as clearly fulfilled since  $\text{Im}g_{t_{2u}}^0(E)$  is not small when  $Q_{t_{2u}}(E) = 0$ . Therefore,  $\text{Im}g_{t_{2u}}(E)$  in Eq. (6) has weight not only when the denominator almost vanishes around  $E = E_R$  but also for energies where the numerator has an appreciable magnitude. Thus, even if  $\text{Im}g_{t_{2u}}(E)$  has a broad peak at the resonance energy, there is also a considerable weight at lower energies. From Fig. 5 this can easily be related to the appreciable magnitude of  $\text{Im}g_{t_{2u}}^0$  in the same energy range. Thus, the different shape of the DOS for  $t_{2u}$  as compared to the other two symmetries can be traced back to the difference in the imaginary part of the associated Green's functions for the host.<sup>21</sup> This, in turn, is related to the host DOS. The  $f$  bands formed from the  $5f$  levels of Ir are, however, situated far above the Fermi level. The host  $f$  states entering, for instance, Eq. (7) are instead originating from tails of the  $d$  states from the atoms surrounding the impurity. This is clear from Fig. 6 where the local unperturbed  $t_{2u}$  DOS is shown together with the DOS of the  $d$  states for the iridium metal. From a similar analysis for the  $a_{2u}$  and  $t_{1u}$  states, it is found that the cause of the

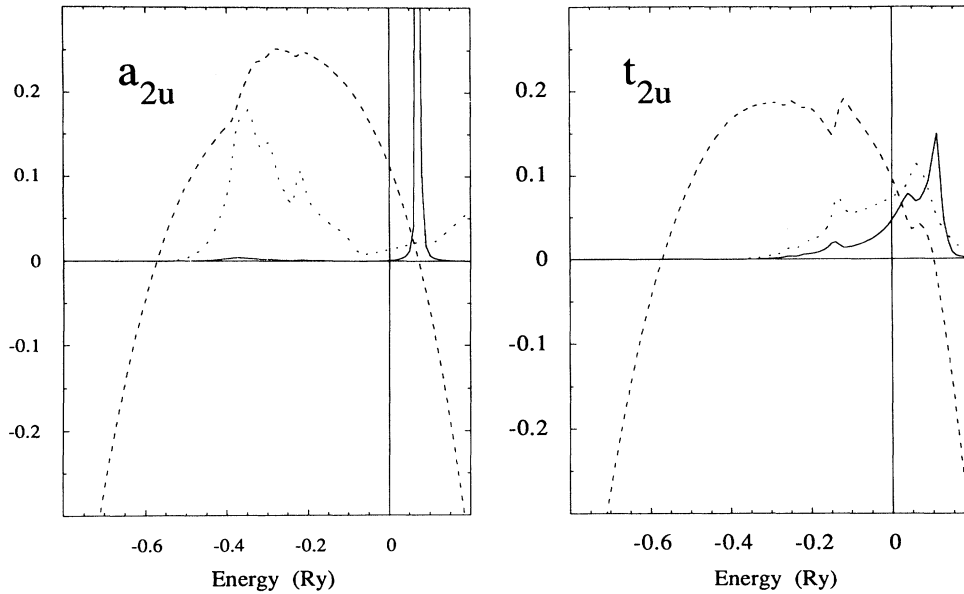


FIG. 5. The functions  $Q_\alpha(E)$  (dashed line),  $x \text{Im} g_\alpha^0(E)$  (dotted line), and  $y \text{Im} g_\alpha(E)$  (solid line) ( $y=1 \text{ Ry}$ ) for  $\alpha=a_{2u}$  ( $x=1000 \text{ Ry}$ ) and  $\alpha=t_{2u}$  ( $x=100 \text{ Ry}$ ). The Fermi level is at zero energy.

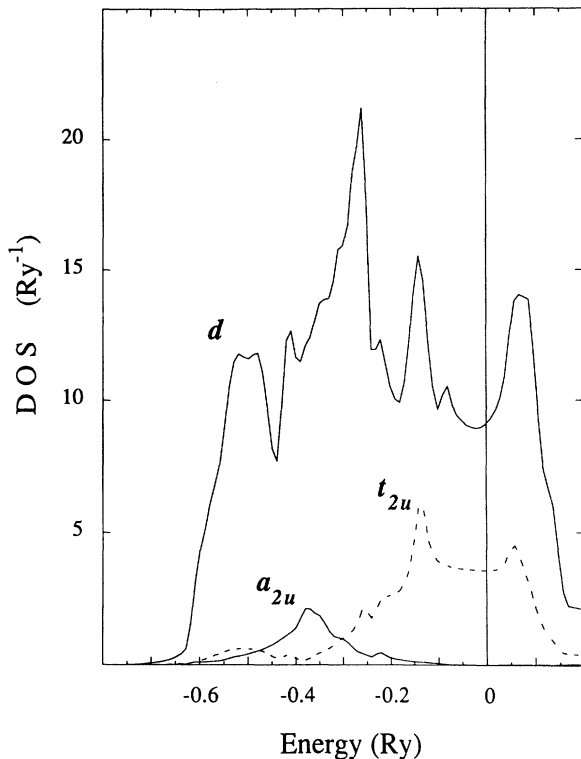


FIG. 6. The  $d$  and  $f$  DOS for the cubic symmetry representations  $a_{2u}$  and  $t_{2u}$ , for Ir metal. The  $f$  DOS are magnified with a factor 10. The Fermi level is at zero energy.

difference between the symmetry representations of the occupied host  $f$  states are that, while the  $t_{2u}$  states originate from tails of wave functions in the antibonding part of the  $d$  bands, the  $a_{2u}$  and  $t_{1u}$  states originate from tails in the low-lying bonding part. Since the cerium  $4f$  level lies in the energy region of the antibonding iridium states, the Ce  $4f(t_{2u})$  states become heavily influenced by the ligand, while the Ce  $4f(a_{2u}, t_{1u})$  states only become slightly broadened. For the case of cerium as an impurity in an early transition-metal host, the  $4f$  level will lie in the energy region for bonding host  $d$  states and therefore we expect a completely reversed influence from the ligand on the Ce  $t_{2u}$ ,  $a_{2u}$ , and  $t_{1u}$  states.

Hence, the fact that, for the present case, the  $t_{2u}$  states do not form a sharp resonance as the  $a_{2u}$  and  $t_{1u}$  states do is due to a strong hybridization with the  $d$  states of the neighboring iridium atoms. For Ce and Pr this hybridization is responsible for the fact that the DOS at the Fermi energy is low enough to ensure a stable nonmagnetic solution. For the heavier lanthanides with larger  $f$  occupancy, the resonance, i.e., the  $a_{2u}$  and  $t_{1u}$  states, starts to become filled and therefore the  $4f$  DOS at the Fermi level becomes large, giving rise to the formation of a magnetic moment. In the following section we investigate more carefully the nature of these magnetic moments.

## V. LOCAL MAGNETIC MOMENTS

As already stated, local magnetic moments of primarily  $f$  character form at the sites of Nd and Pm when they are impurities in an Ir host. However, the nature of these magnetic moments needs further clarification. The re-

sults of Sec. III give a picture of a spin-only  $4f$  magnetic moment where hybridization, between the  $4f$  states of the lanthanide atom and the  $5d$  states of the surrounding host atoms, is present in a similar way as discussed in the previous section. Another possibility could be a standard rare-earth magnetic moment with Russel-Saunders coupling, i.e., the  $4f$  states are of atomic type with very little hybridization with conduction-band states.

In order to allow for this type of solution, which in the LDA is impossible to achieve directly, we will allow for the so-called orbital polarization.<sup>16</sup> Each  $f$  orbital on the lanthanide site is shifted with an amount  $-E^3 m L_\sigma$ . Here  $E^3$  is the Racah parameter,  $m$  the magnetic quantum number, and  $L_\sigma$  the expectation value of the angular momentum, i.e., the orbital moment, for spin  $\sigma$ . From the definition of the Racah parameter,  $E^3$  is calculated as a sum of Slater integrals, which, in turn, are integrals of the radial  $f$  wave function over the atomic sphere.

It is possible to show that when the local DOS at the Fermi level is high enough it is favorable for the system to form orbital moments. This formation involves symmetry breaking, at least in the present form of the splitting term, since the quantum number  $m$  stems from the spherical symmetry in the atomic limit. The Hamiltonian does not have cubic symmetry when  $L_\sigma$  differs from zero and the use of the irreducible representations of the cubic point group  $O_h$  is no longer correct. Instead, the full matrix equation, Eq. (4), is solved and its size is still manageable within the one-site approximation.

For both Nd and Pm, an orbital splitting is obtained in the calculations, but only for the majority spin. The calculated orbital and spin moments are given in Table VI. As can be seen from the table, apart from the existence of orbital moments, the results are very close to the results of the spin-polarized calculations in Table III. Since no spin-orbit coupling is included in the calculation, the relative direction of the spin and orbital moments is undecided, but an antiparallel aligning is chosen in accordance with what the spin-orbit coupling would favor.

We now have a qualitative picture of large, atomic-like, magnetic moments on the rare-earth site resembling a localized  $4f$  shell. But quantitatively the calculated spin

and orbital moments are reduced compared to the free-ion values, i.e., the values obtained from Hund's first and second rules. This deviation can be attributed to an instability of the  $4f$  shell induced by the hybridization with the host  $d$  states. However, considering the limitations of LDA in describing a correlated  $4f$  shell, this deviation may also be ascribed to as due to the approximations adopted in the calculations. Still, we want to point out that the reduction is larger for Nd than for Pm. Therefore, in the case of an instability, it should be more clearly observed for Nd than for Pm.

## VI. SUMMARY AND CONCLUSION

We have performed calculations of the electronic structure and the magnetic properties for the case of light lanthanide ions dissolved in the small-volume transition-metal host iridium. The results show that, for the case of cerium and praseodymium, the impurity is nonmagnetic while for neodymium and promethium the lanthanide ion has both large spin and orbital magnetic moments. This is in good accordance with experiment. The fact that no magnetic moments are formed on the lanthanide atoms, Ce and Pr have been explained in terms of a strong hybridization between the  $f_{12u}$  states of the impurity and the  $5d$  states of the surrounding Ir atoms. For the heavier atoms, Nd and Pm, large magnetic moments are formed due to the substantial local  $4f$  density of states at the Fermi level. In the calculations, these moments are not completely saturated to their maximum possible values. Whether this is due to an instability of the Russel-Saunders coupled  $4f$  shell caused by hybridization, or if it should be attributed to limitations of the approximations used in the calculations, is not clear. Further theoretical and experimental work is needed to clarify the nature of Nd and Pm impurities in iridium metal.

The main result of our investigation is that cerium and praseodymium are found to be nonmagnetic when dissolved in iridium. However, a striking fact is that only a part of the  $f$  states is involved in the hybridization which makes the nonmagnetic solution stable. The rest have a very narrow resonance form which indicates that they are almost bound (virtual bound) states. Although the calculations are only valid for the ground state, one might speculate about the possibility to identify these virtual bound states situated just above the Fermi level as excitations. Since these excitations are likely to be spin polarized, they would increase the entropy and could cause a reentrance of magnetic moments at elevated temperatures.

The fact that we have found a pronounced difference between  $f$  states belonging to different representations of the cubic point group is interesting since electronic structure calculations of transition-metal impurities in various hosts have not reported any significant crystal-field splitting.<sup>4</sup> It is also interesting to speculate whether the extra ordinary crystal-field splitting found in the present calculations also occurs in other similar systems. We intend to study other cerium systems to investigate if the mechanism proposed here has a more general validity.

TABLE VI. Occupation numbers ( $n_i$ ) and charge ( $q$ ) for the impurity atoms together with  $f$ -projected ( $f$ ) and total (tot) spin ( $M$ ) and orbital ( $M^{\text{orb}}$ ) magnetic moments for Nd and Pm. The charge is in units of  $e$  and the magnetic moments are in units of  $\mu_B$ .

Atom	Nd	Pm
$n_{sp}$	0.747	0.816
$n_d$	1.825	1.744
$n_f$	3.035	4.050
$q$	0.417	0.389
$M_f$	1.693	3.132
$M_f^{\text{orb}}$	-3.180	-4.837
$M_{\text{tot}}$	1.720	3.193
$M_{\text{tot}}^{\text{orb}}$	-3.181	-4.837

Finally, we would like to stress that the main purpose of this report was to show that *ab initio* calculations within LDA are capable of arriving at a ground state in accordance with experimental results. However, we do not want to give the impression that this treatment is in any sense complete. Being essentially a mean-field theory, it suffers from the same limitations as the Hartree-Fock solution to the Anderson Hamiltonian.

#### ACKNOWLEDGMENTS

The project was performed with financial support from the Swedish Natural Science Research Council. Valuable help regarding the LMTO–Green’s-function method have been given by Dr. Axel Svane and Dr. Olle Gunnarsson. The hospitality of Professor O. K. Andersen and his group at Max Planck Institute, Stuttgart, where parts of the work was done, is gratefully acknowledged.

- 
- <sup>1</sup>P. W. Anderson, *Phys. Rev.* **124**, 41 (1961).  
<sup>2</sup>For references see, for instance, *Theory of Heavy Fermions and Valence Fluctuations*, edited by T. Kasuya and T. Saso (Springer-Verlag, Berlin, 1985).  
<sup>3</sup>A. M. Tselick and P. B. Wiegmann, *Adv. Phys.* **32**, 453 (1983).  
<sup>4</sup>R. Podloucky, R. Zeller, and P. H. Dederichs, *Phys. Rev. B* **22**, 5777 (1980).  
<sup>5</sup>N. Stefanou, A. Oswald, R. Zeller, and P. H. Dederichs, *Phys. Rev. B* **35**, 6911 (1987).  
<sup>6</sup>V. I. Anisimov, V. P. Antropov, A. I. Liechtenstein, V. A. Gubanov, and A. V. Postnikov, *Phys. Rev. B* **37**, 5598 (1988).  
<sup>7</sup>J. W. Allen and R. M. Martin, *Phys. Rev. Lett.* **49**, 1106 (1982); M. Lavagna, C. Lacroix, and M. Cyrot, *Phys. Lett.* **90A**, 210 (1982).  
<sup>8</sup>B. Johansson, *Philos. Mag.* **30**, 469 (1974).  
<sup>9</sup>D. Glötzel, *J. Phys. F* **8**, L163 (1978).  
<sup>10</sup>W. E. Pickett, A. J. Freeman, and D. D. Koelling, *Phys. Rev. B* **23**, 1266 (1981).  
<sup>11</sup>D. Riegel, H. J. Barth, M. Luszik-Bhadra, and G. Netz, in *Valence Instabilities*, edited by P. Wachter and H. Boppert (North-Holland, Amsterdam, 1982), p. 497; D. Riegel, *J. Magn. Magn. Mater.* **52**, 96 (1985).  
<sup>12</sup>R. Zeller and P. H. Dederichs, *Physica B* **130**, 34 (1986).  
<sup>13</sup>H. J. Barth, M. Luszik-Bhadra, and D. Riegel, *Phys. Rev. Lett.* **50**, 608 (1983).  
<sup>14</sup>L. Büermann, H. J. Barth, K. H. Biedermann, M. Luszik-Bhadra, and D. Riegel, *Phys. Rev. Lett.* **56**, 492 (1986).  
<sup>15</sup>L. Nordström, B. Johansson, and O. Eriksson, *Phys. Scr.* **39**, 394 (1989).  
<sup>16</sup>M. S. S. Brooks, *Physica B* **130**, 6 (1985); O. Eriksson, M. S. S. Brooks, and B. Johansson, *Phys. Rev. B* **41**, 7311 (1990).  
<sup>17</sup>O. Gunnarsson, O. Jepsen, and O. K. Andersen, *Phys. Rev. B* **27**, 7144 (1983); O. K. Andersen, Z. Pawłowska, and O. Jepsen, *ibid.* **34**, 5253 (1986).  
<sup>18</sup>O. K. Andersen, *Phys. Rev. B* **12**, 3060 (1975).  
<sup>19</sup>P. Villars and L. D. Calvert, *Pearson’s Handbook of Crystallographic Data for Intermetallic Phases* (American Society for Metals, Ohio, 1986).  
<sup>20</sup>U. von Barth and L. Hedin, *J. Phys. C* **5**, 1629 (1972).  
<sup>21</sup>In the orthogonal LMTO representation (Ref. 17)  $g^0(E)$  is changed when the local representation  $\gamma$  is altered during the iterations. The relation between  $g^0$  in the representation of the pure host  $\gamma^0$  and in the representation appropriate for the perturbed system  $\gamma^{\text{imp}}$  is  $g^0(\gamma^{\text{imp}}) = [p g^0(\gamma^0) - \gamma^0 + \gamma^{\text{imp}}] p$ ,  $p = P^0(\gamma^0)/P^0(\gamma^{\text{imp}})$ , where  $P^0(\gamma^{\text{imp}})$  and  $P^0(\gamma^0)$  are the unperturbed potential functions in the two representations  $\gamma^{\text{imp}}$  and  $\gamma^0$ , respectively. It is  $g^0(\gamma^{\text{imp}})$  that enter Eq. (6) and the discussions that follow.